Analysis of Capacitance Measurements on Silicon Microstrip Detectors

E. Barberis, N. Cartiglia, J. Dann, T. Dubbs, K. Noble, K. O'Shaughnessy, J. Rahn, H. F.-W. Sadrozinski, R. Wichmann
SCIPP, University of California, Santa Cruz, CA 95064
T. Ohsugi, *Hiroshima University, Higashi-Hiroshima 724, Japan*
Y. Unno, *KEK, Oho 1-1, Tsukuba, Ibaraki 305, Japan*
H. Miyata, *Niigata University, Niigata 950-21, Japan*
N. Tamura, *Okayama University, Okayama 700, Japan*
K. Yamamoto, *Hamamatsu Photonics K.K., Hamamatsu City, Japan*

Abstract

We present an analysis of the total strip capacitance of double-sided, AC-coupled silicon microstrip detectors. We evaluate the radiation hardness and the noise contribution of different strip geometries. We comment on a serious failure mode.

I. Introduction

For silicon microstrip detectors, the total strip capacitance is a major contributor to the amplifier noise. We have shown before [1], that in general, geometric considerations determine the values of the capacitances: narrow strip implants and wide p+ blocking strips (on the ohmic side) minimize the interstrip and coupling capacitance[2,3]. The extraction of the capacitances from LCR measurements is complicated by the frequency dependence of the measurements. With help of a comprehensive SPICE simulation, frequency independent capacity values can be determined[4].

We have previously measured the effect of proton and gamma radiation on the total capacitance[1]. We now determined the noise of microstrip detectors of various geometries and with different radiation history and extracted values for the capacitances. These results are compared with the direct LCR measurements.

II. Experimental Set-up

We have measured the interstrip, coupling and body capacitance as function of strip and p-blocking implant width. Single-sided AC-coupled test detectors of various geometries were manufactured by Hamamatsu Photonics [5] in a program to determine the optimum geometric layout of double-sided silicon detectors for the SSC [6]. Details can be found in refs. [4,7]. Based on our findings, double-sided prototypes of 6cm length were produced with 12μm implant, 10μm metal and 24μm p^+ blocking strips [6].

The capacitance measurements on biased detectors have been performed as function of frequency with a HP 4284A LCR meter. The measured capacitances exhibit a strong frequency dependence due to the fact that the detectors act as an extended network of resistors and capacitors. With SPICE simulations we extract frequency independent capacitance and resistance values. A more complete description of the simulation and the results is given in ref. [7].

The noise was determined using a low power, low noise amplifier-comparator VLSI circuit with 32ns shaping time [8] and a digital pipeline chip [9], both developed for the LPS in ZEUS [10]. From the dependence of the counting rate on the threshold voltage the equivalent noise charge (ENC) can be extracted and the capacitance calculated.

III. Body Capacitance

We have presented before [1,4] the extraction of the coupling and interstrip capacitance. We report here on the body capacitance which is important to determine the depletion voltage in C-V plots.

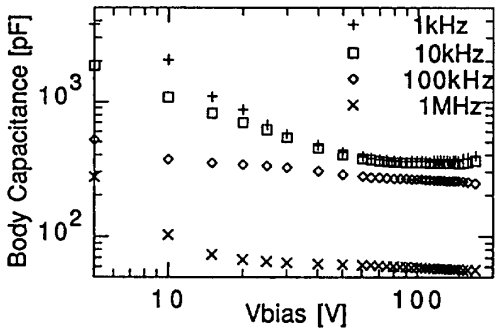

Fig. 1 C-V plot of the p-side Hamamatsu test structure

Fig. 1 shows the C-V plot of the Hamamatsu test structure for several frequencies, taken between the biasing bus and the backplane. The data suggests that at higher frequencies the simple two-component analysis of the LCR meter does not describe the complexity of the circuit. On the other hand, the body capacitance above depletion can be well descibed by a SPICE simulation which includes biasing resistors and the capacitance of the guard ring (Fig. 2).

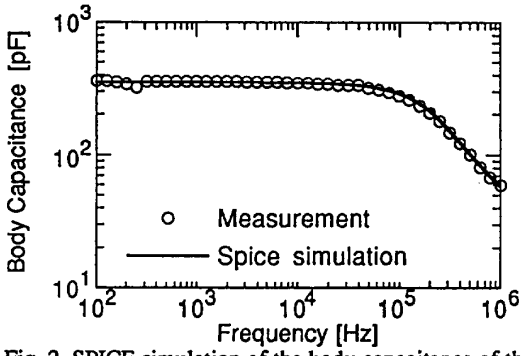

Fig. 2 SPICE simulation of the body capacitance of the p-side Hamamatsu test structure

Novel designs of detectors with varying strip pitch p and/or width w ("wedged" detectors, see ref. [11]) pose the question of how depletion voltage and body capacitance depend on the strip geometry. We have investigated this dependence using explicit analytic expressions for the field [1,12]. Assuming a detector of thickness d, strip width w and w' of p-side and n-side, respectively and depletion voltage V_{D0} as a planar diode, we find that both the strip detector depletion voltage:

$$V_D = V_{D0}\{1+2\frac{p}{d}[f(\tfrac{w}{p})+f(\tfrac{w'}{p})]\} \quad (1)$$

and the body capacitance per unit length at depletion:

$$c_D = \varepsilon\frac{p}{d+p\cdot[f(\tfrac{w}{p})+f(\tfrac{w'}{p})]} \quad (2)$$

are dependent on an universal function f(w/p). Numerically:

$$f(x) = -1.11\cdot10^{-3}x^{-2}+5.86\cdot10^{-2}x^{-1}+0.240 \\ -0.651x+0.355x^2, x = w/p \quad (3)$$

IV. Total Capacitance

The total strip capacitance is the sum of the measured AC interstrip capacitance to the first two pairs of neighbors, a small correction of about 10% due to all the remaining strips, and the body capacitance.

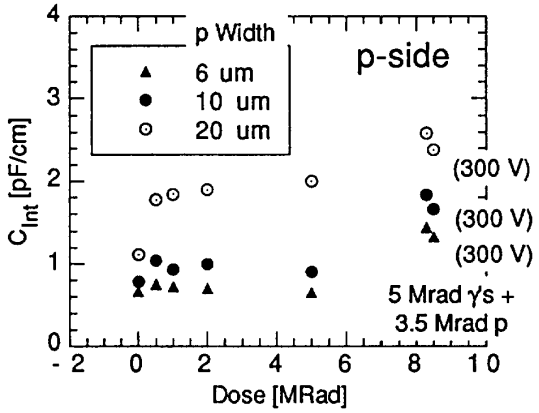

Fig. 3 Interstrip capacitance for p-side test structures.

For unirradiated detectors, we observe somewhat higher capacitances on the ohmic side (Fig. 4) than on the junction side (Fig. 3) [1], suggesting the presence of free charges close to the surface which can be removed only with increased electric fields. This explanation is supported by the fact that the ohmic side interstrip capacitance continues to decrease with increasing bias voltage, even after depletion is reached.

V. Radiation Damage

We have irradiated the sample detectors with gamma rays from a ^{60}Co source and with 650 MeV protons with total doses of up to 8.5 MRad [13,14]. Here we will only discuss the change in interstrip capacitance. The coupling capacitance was shown to be stable[14] and the bulk effects leading to a change in the depletion voltage are discussed in Ref. [15].

We determined the AC interstrip capacitance to the next four neighbors for both the junction and ohmic side as a function of the total dose, choosing the high frequency limit at 1 MHz (cf. Ref. [1].). The results are shown for the p-side in Fig. 3 for different p-implant width. First we collected a gamma dose of 5 MRad. We see that the interstrip capacitance is nearly constant for small strip width and increases with radiation for wide strip width (20μm). After gamma irradiation, we added protons with a fluence of about 10^{14} p/cm^2 for a total dose of 8.5 MRad. During the proton irradiation, the n-bulk inverted[16], causing the junction to move to the n-side: depletion is now starting from the n-side. We conclude from Fig. 3 that the interstrip capacitance is about doubled after inversion and moreover exhibits a dependence on the bias voltage: when we raise it from 200 V (the depletion voltage) to 300 V, the capacitance decreases. This voltage dependence is similar to the interstrip capacitance on the ohmic side before irradiation, which we attributed to insufficient removal of all free charges between the strips.

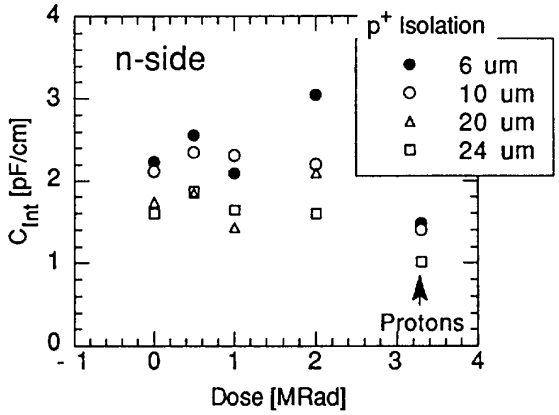

Fig. 4 Interstrip capacitance for n-side test structures of 10μm width.

In Fig. 4, we show the interstrip capacitance for the n-side for different p^+ blocking strip widths and n-implant width of 10 μm as function of γ dose and for a separate proton irradiation with 10^{14} p/cm^2. We find that the n-side interstrip capacitance is constant during gamma irradiation, at least for wide p^+isolation width. After inversion, i.e., after proton irradiation, the interstrip capacitance is reduced for all geometries to below the pre-rad levels. Moreover, no dependence on the bias voltage is observed, very much like on the p-side before inversion. These facts are consistent with our hypothesis that on the ohmic side, insufficient removal of free charges in low electric fields causes an increase in interstrip capacitance.

VI. Noise

We have measured the noise of a low noise amplifier-comparator chip [8] as function of capacitance with both discrete capacitors and silicon strip detectors of different width.

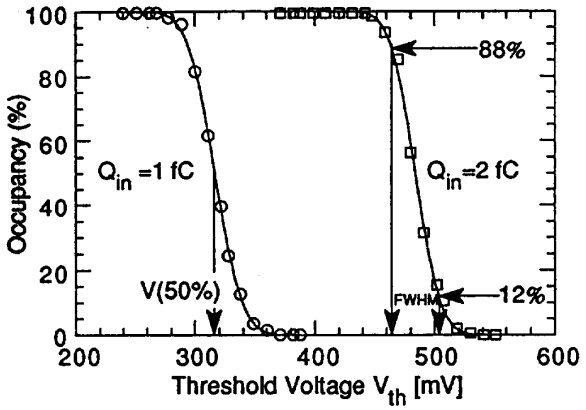

Fig. 5 Determination of the noise using the calibration signal. The noise FWHM is the difference in threshold voltage between the 80% and 12% occupancy points.

Fig 5 shows the calibration method used to extract the noise value. Two input charges of 1fC and 2fC are injected and the synchronous counting rate (occupancy) recorded as function of threshold voltage Vth. The threshold voltage difference of the 50% points is the gain in mV/fC, and the width of the threshold curves gives the noise. Specifically, the threshold voltage difference between the 88% and the 12% occupancy points is equal to the noise FWHM. We actually fit the data with an error function to extract the noise sigma. Fig. 6 shows the noise of the amplifier as function of load capacitance. In one case, the capacitances are given by external discrete components, while in the other they are presented by p-strips of different width, whose capacitance values can be calculated with the help of Fig. 3. The two noise curves are nearly identical, which leads us to conclude that the total strip capacitance generates noise like a discrete capacitor. The resistance of the metal strip (30 Ω/cm for 10μm width) does not contribute significantly to the noise of the fast amplifier.

We have irradiated p-type test detectors in the TRIUMF proton beam of 500 MeV with a fluence of $1.5*10^{13}$p/cm^2, which leaves the samples close to type inversion. Both the capacitances and the noise values increased during irradiation. The noise σ_n is of the form:

$$\sigma_n = \sqrt{(\sigma_0 + 40 \cdot C)^2 + F\frac{2 \cdot i \cdot \tau}{e}} \text{ [electrons] }, \qquad (4)$$

where σ_0 is the noise of the amplifier without load (about 800 e$^-$) and the capacitance values C are derived from Fig 3. The second term in eq. 4 is contributed by the shot noise of the current i and is about 426 electrons for this fluence. F is a function depending on the shaping of the preamp and is F=1.16 for our preamplifier with rise time τ=32ns. We have included these increased capacitance and noise values in Fig. 6.

Table I
Capacitances extracted from LCR Measurements and Calibration Noise for Hamamatsu p-side test structures

$p-width$ [μm]	$Fluence$ [cm^{-2}]	C_{LCR} [pF]	C_{Noise} [pF]
6	0	5.5	3.2
6	$1.5 \cdot 10^{13}$	10	9.3
10	0	6,1	5.0
10	$1.5 \cdot 10^{13}$	12	11.3
20	0	8.2	4.0
20	$1.5 \cdot 10^{13}$	15.9	15.4
30	0	11.3	9.3
30	$1.5 \cdot 10^{13}$	≈ 22	21.9

In Table I, we list the values of the capacitances of the different strip geometries measured directly with the LCR meter and determined from the calibration noise, before and after proton irradiation. The post-rad value of C_{LCR} for 30μm width is an estimate, because the proton data are missing. The agreement for small capacitances is only fair because according to eq. 4, the noise measurement is then not sensitive to the capacitance. For larger capacitances, the agreement is good.

An alternative method to determine the noise σ is to determine noise rates (occupancy in 10MHz time slices) as function of the square of the threshold voltage of the amplifier.

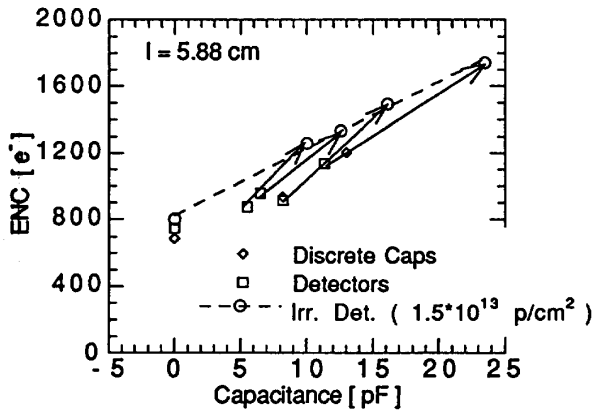

Fig. 6 Noise as a function of capacitance. The arrows connect the pre-rad and post-rad noise and capacitance values for the same strip.

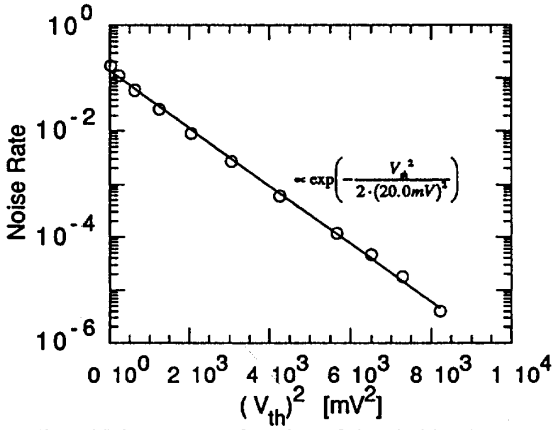

Fig. 7 Noise rate as a function of threshold voltage V_{th}.

discriminator. Fits of the form

$$N = N_0 \cdot e^{\frac{V_{th}^2}{2\cdot\sigma_n^2}} \quad (5)$$

give the noise σ_n directly. An example is given in Fig. 7 which displays the exponential nature of the noise rate of an disconnected preamp channel. The slope of the noise rate curve gives σ_n=20.0mV, while the calibration method yields σ_n=19.3mV, indicating good agreement between the two methods.Capacitances can be extracted from σ_n using eq. 4 with values for σ_0 determined seperately for every detector.

In Table II, we show noise rates for the p-type Hamamatsu test structures determined in three different ways: calculated from the LCR capacitance measurements, measured with the calibration and measured with the noise rate in a threshold scan. While the first two agree quite well, we see that the threshold scans give larger noise values: they sample the noise rate at larger threshold values and thus are sensitive to low-rate, but high amplitude contributions to the noise. We can attribute this noise component to the fact that there is an occasional breakdown of the junction due to the exact overlap of the p-implant and the metal strip, termed "popcorn noise" by T. Ohsugi[6].

Table II
Equivalent Noise Charges from LCR Measurements, Calibration Noise and Threshold Scans for p-side Hamamatsu Test Structures after a Fluence of $1.5*10^{13}$p/cm^2

$p-width$ [μm]	$ENC[e^-]$ $calc:LCR$	$ENC[e^-]$ $Cal.Noise$	$ENC[e^-]$ $Thresh.Scan$
6	1286	1258	1725
10	1361	1333	1542
20	1510	1492	1613
30	≈1746	1742	1875

We also have investigated the noise of the Hamamatsu double-sided prototype detectors (DSSD) of 6cm length. Here the implants are made 2μm wider than the metal to prevent breakdown. We performed noise rate measurements before and after proton irradiation with a fluence of about $5*10^{13}$p/cm^2 (Fig.8). The current per strip amounted to about i=1.6μA, leading to a noise contribution of about 862 electrons.

In Table III, we compare the total capacitances as determined with LCR measurements (from Figs. 3 and 4, for 10μm strips and 24μm p^+ blocking implants on the ohmic side), and from noise rate measurements (eqs. 4 and 5), respectively. We also bonded two non-adjacent strips together to measure the noise on 12cm long strips after irradiation. The general agreement between LCR measurements and noise rate determination is fairly good, indicating that the inverted detector appears stable, in contrast to the p side of the 6cm long unirradiated detector, where we possibly are observing slight breakdown. An interesting fact mentioned above is that after inversion, the capacitance on the p-side becomes bigger than the n-side capacitance, while before inversion it is the other way around. Also, the n-side capacitance drops below its pre-rad level. We can see both trends in our data (Table III). In addition, the capacitance of 6cm and 12cm long detectors scale reasonably well.

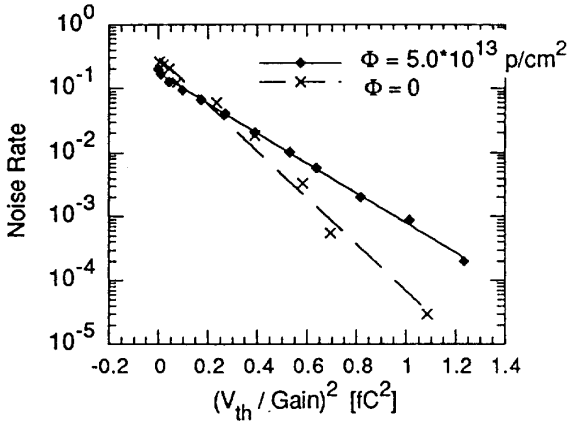

Fig. 8 Noise rate as a function of threshold V_{th}. for the 6cm long p-side strips of the DSSD prototype before and after a proton fluence of $5*10^{13}$ p/cm^2.

Table III
Capacitances extracted from LCR Measurements and Threshold Scans for Hamamatsu DSSD

n/p	$Length$ [cm]	$Fluence$ [$10^{13} p/cm^2$]	C_{LCR} [pF]	C_{noise} [pF]
p	6	0	6.6	11.7
p	6	5	13.2	14.0
p	12	5	26.4	27.7
n	6	0	11.5	12.8
n	6	5	7.8	8.4
n	12	5	15.6	23.3

VII. FAILURE MODES

For the future, very large silicon tracking systems are proposed[17]. Failure modes are important because of the large scale integration of detectors and electronics. We have identified as one specially worrisome failure mode the breakdown of one of the coupling capacitors, shorting the p- or n-implant to the input of the amplifier. Given the fact that we plan to bias both the junction and the ohmic side, this will short the amplifier chip to the bias voltage of up to 100 V via the biasing resistor.

We have tested this failure by breaking a coupling capacitor on one of the p-side Hamamatsu test structures (implant width = 30μm) and measuring noise and gain on the channel with the shorted capacitance and the next neighboring channels. Again, the bipolar "TEKZ" amplifier-comparator chip of Ref.[8] was used. We kept the total bias voltage of the

detector at 100V, but changed the negative voltage on the p-side biasing ring. Fig 9 shows the i-V curve of the current I_{Amp} absorbed into the amplifier as function of the p-side bias voltage. At about -6V, the amplifier channel connected to the shorted capacitor stopped working. A current in excess of 3μA switches the pre-amp off. This was completely reversible, both gain and noise reached their original values whenever the p-side bias voltage was turned to zero. Yet, the amplifier was able to absorb currents in excess of 300μA.

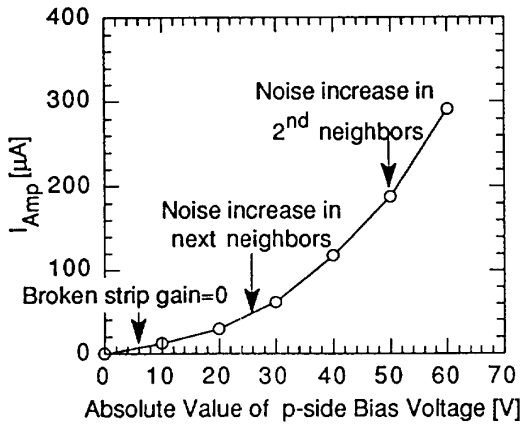

Fig. 9 Current into the amplifier of the shorted capacitor as function of p-side bias voltage.

The next neighbors showed increased noise at about -25V and the second neighbors showed increased noise at -50V, while preserving the normal gain. This noise increase was the only effect we were able to observe on the readout chips. We then illuminated the strips with a laser of about 10μm spot size[18] and realized that in addition, strips are shorted together via the "punch through effect"[19]: if a threshold voltage between strips is reached, current flows to keep this threshold voltage approximately constant. With a bias voltage of above -25V, the voltage difference between the strip with the broken capacitor, which is held at 0V, and its neighbors reaches the threshold voltage and thus the three strips get shorted together. We see an increase in current, which is now supplied via three biasing resistors. When the biasing voltage reaches -50V, the next pair of neighbors gets shorted to the first pair, thus increasing the current into the amplifier via their biasing resistors and increasing the noise in those strips. We can expect that for a bias voltage of -100V, about 9 strips will be shorted together. This value depends on the strip geometry, because the punch through voltage depends on the strip separation: we expect larger voltage differences and fewer shorted strips for narrower strips. Note that at -60V, a current of 300μA is absorbed in the amplifier chip, yet we observed normal gain and noise numbers on all channels but the few neighbors, affected by the punch through.

VIII. CONCLUSIONS

We have measured the body capacitances of AC-coupled silicon strip detectors. The frequency dependence of the measurement can be simulated with SPICE and is understood in terms of a network of distributed capacitors and resistors.

We have derived the dependence of the depletion voltage and body capacitance on the strip pitch and width of strip detectors.

With a fast, low-noise amplifier, we determined the noise of detectors of different geometries and radiation histories and extracted the capacitance. which in general agrees with the capacitance measured with an LCR meter. Noise rate measurements in a threshold voltage scan allow the detection of low-rate, high-amplitude noise components.

We investigated a failure mode of DSSD, the breakdown of coupling capacitors. We find that a bipolar preamplifier limits the consequences to the shorting together of a few strips via the punch through effect.

IX. ACKNOWLEDGEMENTS

We thank W.A. Rowe, E. Spencer, A. Webster and M. Wilder for technical help and fruitful discussions. This work is supported in part by the US. Department of Energy, the Texas National Research Laboratory Commission and the US-Japan Collaborative Program and the Joint Research of the International Scientific Research Program, Ministry of Education, Science and Culture, Japan.

X. REFERENCES

[1] E. Barberis *et al.*, Capacitances in Silicon Microstrip Detectors, SCIPP 93/16, presented at the International Symposium on Development and Application of Semiconductor Tracking Detectors at Hiroshima, Japan, May 22-24, 1993.

[2] R. Sonnenblick *et al.*, Electrostatic Simulations for the Design of Silicon Strip Detectors and Front-end Electronics, Nucl. Instrum. Methods **A310** (1991) 189.

[3] R. Yamamoto, Proceedings of the SDC Collaboration Meeting at KEK, SDC-91-33, May 1991.

[4] E. Barberis et al., Measurement of Interstrip and Coupling Capacitances of Silicon Microstrip Detectors, IEEE Nucl. Sci. Symp., Orlando FL, 1992, SCIPP 92/14.

[5] Hamamatsu Photonics K.K., Hamamatsu City, Japan.

[6] T. Ohsugi *et al.*, Double-sided Sensors for SDC, presented at the International Symposium on Development and Application of Semiconductor Tracking Detectors at Hiroshima, Japan, May 22-24, 1993.

[7] C. LeVier, Capacitance in Silicon Strip Detectors, UC Santa Cruz Senior thesis, SCIPP 92/26.

[8] E. Barberis *et al.*, A Low-Power Bipolar Amplifier Integrated Circuit for the ZEUS Silicon Strip System, Nucl. Phys. B (Proc. Suppl) **32** (1993).

[9] J. DeWitt, The Time Slice Chip, Nucl. Instrum. Methods **A288**, 209 (1990).

[10] K. O'Shaughnessy *et al.*, Testing and Installation of ZEUS LPS Detector Planes, presented at the International Symposium on Development and Application of Semiconductor Tracking Detectors at Hiroshima, Japan, May 22-24, 1993.

[11] J. Krismanic *at al.*, Wedged Detectors, *ibid.*

[12] J. Rahn, Depletion Characteristics of Silicon Microstrip Detectors, SCIPP 93/12.

[13] H. Ziock *et al.*, Measurement of Proton Induced Radiation Damage to CMOS Transistors and PIN Diodes, IEEE Trans. Nucl. Sci. **37**, 1238 (1990).
[14] D. Pitzl *et al.*, Study of Radiation Effects on AC-coupled Silicon Strip Detectors, Nucl. Phys. B (Proc. Suppl.) **23A** (1991) 340.
[15] H. Ziock *et al*, Temperature Dependence of the Radiation Induced Change of Depletion Voltage in Silicon PIN Detectors, SCIPP 93/40, presented at the International Symposium on Development and Application of Semiconductor Tracking Detectors at Hiroshima, Japan, May 22-24, 1993.
[16] D. Pitzl *et al.*, Type Inversion in Silicon Detectors, Nucl. Instrum. Methods **A311** (1992) 98.
[17] A. Seiden, The SDC Silicon Tracking Device, this Symposium.
[18] E. Barberis *et al.*, A Test Station for Silicon Microstrip Detectors and Associated Electronics, SCIPP 92/60.
[19] J. Ellison *et al.*, Punch-Through Currents and Floating Strip Potentials in Silicon Detectors, IEEE Trans. Nucl. Sci. **36**, (1989) 267.